Numerical investigation of the tip leakage vortex of an isolated plate/airfoil T-junction with gap

D. Lamidel[1,2,3] *- G. Daviller*[2] *- M. Roger*[1] *- H. Posson*[3]

[1]LMFA, UMR CNRS 5509, École Centrale de Lyon, 69134 Écully Cedex, France,
david.lamidel@ec-lyon.fr
[2]CERFACS, 42 Avenue Gaspard Coriolis, 31057 Toulouse Cedex, France
[3]Safran Aircraft Engines, 77550 Moissy Cramayel, France

ABSTRACT

A numerical investigation of the tip leakage flow of a single airfoil is carried out. The configuration consists of a non-rotating, isolated airfoil between two horizontal plates with a gap of 10 mm between the tip of the airfoil and the lower plate. The Mach number is 0.2 and the Reynolds number based on the chord is 9.3×10^5. With the aim of modelling the tip clearance noise, an evaluation of the capacities of the Reynolds-Averaged Navier-Stokes (RANS) and Large Eddy Simulation (LES) methodologies to predict the tip leakage flow is carried out. The mean aerodynamics of the tip leakage vortex is globally predicted by the simulations. The spectral content of the wall pressure fluctuations in the tip region is correctly computed by the LES. The spectral signature of the tip leakage flow is identified and explained by flow detachment using Dynamic Mode Decomposition.

KEYWORDS

Isolated airfoil, Gap, Tip leakage vortex, Large Eddy Simulation, Reynolds-Averaged Navier-Stokes

NOMENCLATURE

Symbols

c	Chord (m)
s	Gap height (m)
β	Angle of attack (°)
Re	Reynolds number (-)
Ma	Mach number (-)
p	Static pressure (Pa)
T	Static temperature (K)
C_p	Pressure coefficient (-)
U, V, W	Mean velocity components

Acronyms

RANS	Reynolds-Averaged Navier-Stokes
LES	Large Eddy Simulation
RMS	Root Mean Square
PS	Pressure Side
SS	Suction Side
LE	Leading Edge
TE	Trailing Edge
PIV	Particule Image Velocimetry
PSD	Power Spectral Density
DMD	Dynamic Mode Decomposition

Subscripts

$_0$	Relative to the reference state
$_{max}$	Relative to the maximum value

INTRODUCTION

The bypass ratio of aircraft turbofan engines tends to increase. It is associated with a reduction of the fan rotation speed, the exhaust jet speed and possibly the nacelle length. Therefore, the fan stage is currently a major source of noise at approach regimes. In this context, the understanding and prediction of secondary noise sources, such as the tip clearance noise in the fan stage, is mandatory.

In the fan stage of turbofan engines, a gap between the tip of fan blades and the casing wall is required. As a consequence, a highly three dimensional unsteady secondary flow develops. The tip leakage flow goes from the pressure side to the suction side of the blade. When the flow leaves the gap, it interacts with the primary flow and rolls up to form the tip leakage vortex. The aerodynamic phenomena are mainly controlled by the blade tip loading, gap height, blade tip thickness, chord length, Reynolds and Mach numbers. The consequences of a too strong gap are the drop of the aerodynamic fan performance and the increase of radiated far field noise (Lakshminarayana 1996).

This increase of the radiated noise from axial fans was first observed experimentally when the height of the gap increased (Longhouse 1978). Therefore, source mechanisms responsible for tip clearance noise generation were investigated. Firstly, Kameier & Neise (1997) have identified a component of the tip clearance noise called the rotating instability. This mechanism consists of coherent vortical structures coming from the tip clearance interact with the fan blades, causing periodic fluctuations of the blade loading, and thus inducing tonal noise in the far field. Yet, as these vortices have a range of tangential velocities, broadband humps are observed instead of sharp tonal peaks. Secondly, Fukano & Jang (2004) studied another mechanism: the interaction of the tip leakage vortex with the blade. The tip clearance noise consists of a discrete frequency noise due to the tip leakage vortex wandering and a broadband noise due to the enhancement of stochastic velocity fluctuations in the blade passage. Recently, Jacob et al. (2010) identified two source mechanisms. Turbulent structures are generated by the detachment of the tip leakage flow on the edge of the pressure side. Then, sound is generated as these structures leave the clearance region either directly or by interaction with the edge of the suction side. In addition, unsteady perturbations, fed by the tip leakage vortex, become sound sources as they are scattered by the trailing edge corner.

To improve existing prediction models or to model new noise sources features, an understanding of the flow physics is first needed. Large Eddy Simulation (LES) is a well-suited tool to investigate the flow phenomenon. Indeed, LES resolves part of the unsteady flow field in regions that are not always accessible with measurements. On the other hand, RANS simulation are often used to compute the mean flow-field and feed analytical modelling of the acoustic sources. The objective of this paper is to evaluate the capabilities of RANS and LES, with respect to experimental data, to compute the aerodynamics of the tip leakage flow. Moreover, regarding the high Reynolds number which characterises the flow in a real turbomachinery configuration, a wall law is required. Therefore, the behaviour of a wall law for the tip leakage flow phenomenon is studied and compared to the wall-resolved LES from Koch et al. (2020). Firstly, the experimental set-up and the numerical approach are presented. Secondly, the flow field of the airfoil-freejet facility is analysed. Next, the incoming flow and the airfoil pressure distribution are studied. Then, the aerodynamics of the tip leakage vortex is considered. Finally, the pressure fluctuations in the tip region are studied.

EXPERIMENTAL SET-UP

A sketch of the experimental set-up considered in this study is shown in Fig. 1a (Jacob et al. 2016). A fixed single airfoil is mounted between two flat plates with a tunable gap between the lower plate and the airfoil tip. Air is coming from a rectangular nozzle. The advantage is that the tip clearance noise contribution to the far field noise is more easily isolated than in a turbomachinery configuration. To ensure a uniform flow, the isolated airfoil is placed into the potential core of the rectangular freejet.

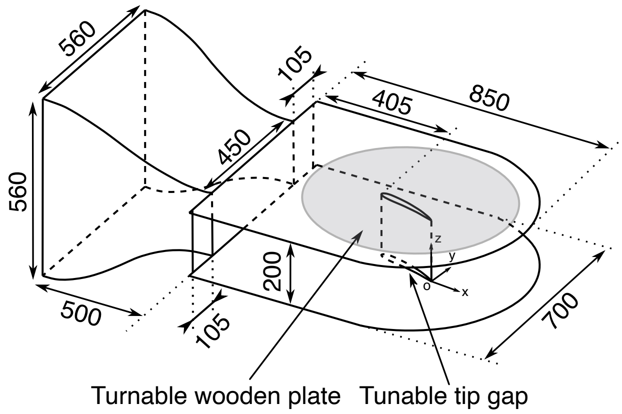

(a)

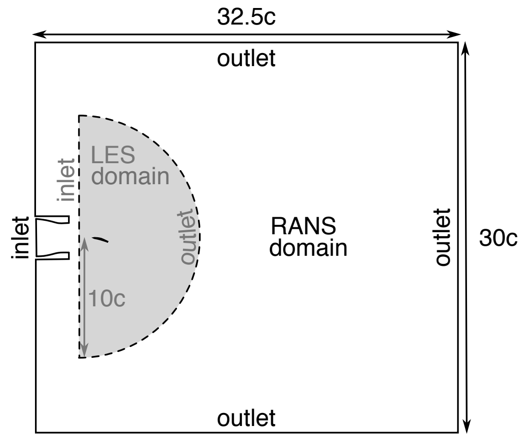

(b)

Figure 1: **(a) Sketch of the experimental set-up. (b) Sketch of the RANS and LES computational domains.**

The airfoil is a NACA 5510 of chord c = 200 mm. The geometrical angle of attack is β = 16.5°. The gap height is s = 10 mm. The mean flow velocity at the exit nozzle is U_0 = 70 m/s, corresponding to a Mach number Ma_0 = 0.20 and a Reynolds number based on the chord $Re_0 = 9.3 \times 10^5$. One chord upstream of the airfoil, the boundary layer thickness on the plate is 6.2 mm. The experiment is carried out under ambient pressure p_0 = 97 700 Pa and ambient temperature T_0 = 290 K.

The coordinate system (o, **x**, **y**, **z**) used in this study is depicted in Fig. 1a. The origin, defined at the trailing edge-tip corner, is more appropriate to study the tip leakage vortex. The **x** axis is in the streamwise direction. The **y** axis is in the crosstream direction, from pressure side to suction side. The **z** axis is in the spanwise direction, from the lower to the upper plate.

COMPUTATIONAL APPROACH

A computational domain accounting for the wind tunnel installation effects is considered (Fig. 1b). Indeed, when testing a lifting airfoil, the main stream is deflected by the equivalent lateral momentum injection, which reduces the effective angle of attack (Moreau et al. 2003). The importance of this interaction depends on the ratio between the jet width and the streamwise projected area of the airfoil. Wang et al. (2009) set up a numerical procedure on the same kind of freejet facility to study airfoil self-noise. A RANS simulation of the whole configuration including the nozzle is carried out. In order to save computational cost, a LES is achieved over a smaller computational domain (Fig. 1b). The RANS solution is used to define the boundary conditions of the LES and also to initialise it.

The RANS computation is carried out using the ***elsA*** software by means of a finite volumes, cell-centered approach to solve the Navier-Stokes equations on a multiblocks structured mesh (Cambier et al. 2013). The computational domain including the nozzle is a rectangular box of dimensions 32.5c $\times$ 30c $\times$ c as sketched on Fig. 1b. The total number of cells is about 28×10^6, split into 622 structured blocks. The wall resolution is $\Delta y^+ < 2$. 60 elements are used to discretise the gap. Total pressure and temperature are imposed at the inlet of the nozzle contraction to get a Mach number of 0.2 at the exit section. The ambient static pressure is imposed at the outlets of the domain. An adiabatic no-slip wall condition is specified for all walls. The Roe flux scheme (Roe 1981) with a second order minmod flux limiter is used. The two-equations turbulence model $k - \omega$ Wilcox (Wilcox 1988) is chosen with the Zheng limiter (Zheng & Liu 1995). A multigrid method with a V-cycle is used to speed up the convergence of the results. A total of 288 processors during 9 hours were used to drop the residual of the energy equation by 5 orders of magnitude.

The LES is performed using ***AVBP***, an explicit, unstructured, massively parallel solver (Schønfeld & Rudgyard 1999). The computational domain depicted in Fig. 1b is a half disk with a radius of 10c, extruded over the whole channel height. The inlet is one chord upstream the airfoil leading edge. The total number of tetrahedrons is approximately 230×10^6. Edge size of the mesh around the airfoil and close-ups are shown on Fig. 2a. A direct approach, computing the sound together with its fluid dynamic source field by solving the compressible flow equations, is achieved. The acoustic propagation zone is also a half disk with a radius of 4c, extruded over the half channel height. The maximum edge size inside the zone is 2 mm leading to a mesh cut-off of 28.3 kHz. The mesh size increases towards the outlet to dissipate acoustic waves and avoid reflexion. 20 elements are used to discretise the gap. The mesh sizes at the wall of the incoming boundary layer and blade tip region are: $\Delta x^+ = \Delta y^+ = \Delta z^+ < 100$ in wall units. As a consequence, a wall-law boundary condition is used to model the boundary layer (Schmitt et al. 2007). A fully non-reflecting inlet boundary condition is used to inject three-dimensional turbulence while still being non-reflecting for outgoing acoustic waves (Daviller et al. 2019). The injected synthetic turbulence is based on Kraichnan (1970). The turbulence spectrum has a Passot-Pouquet expression (Passot & Pouquet 1987). The RMS velocity of the injected turbulent field is the one from the RANS simulation and its most energetic turbulent length scale L_e is 6.3 mm. The latter is computed using a property of the Passot-Pouquet spectrum ($L_e=\sqrt{2\pi}L_t$) and the measured integral length scale L_t (2.5 mm). At the outlet, characteristic boundary condition for the Navier-Stokes equations is used (Poinsot & Lele 1992). The Two-Step Taylor Galerkin C numerical scheme is used (Colin & Rudgyard 2000). It is third order accurate in time and space. The unresolved turbulent contributions are modelled with the SIGMA subgrid scale model developed by Nicoud et al. (2011). The fixed time-step is 3.5 x 10^{-5} c/U_0 corresponding to a CFL number of 0.82. Starting from the RANS simulation, a computational time of 7 c/U_0 was required to leave the transient state. Convergence is monitored with pressure probes in the incoming flow, in the tip leakage vortex and on the airfoil. A total of 4096 processors during 96 hours were used to acquire statistics over 20 c/U_0.

INSTANTANEOUS FLOW

Fig. 2b shows instantaneous iso-surfaces of Q criterion (Q = 2.4 x 10^2 $(U_0/c)^2$) from the LES, colored by the longitudinal vorticity component in the tip leakage flow region. The tip leakage vortex, the tip separation vortex and induced vortices are clearly identified as observed by You et al. (2007). The tip separation vortex in the gap is generated by the separation of the tip leakage flow. The tip leakage vortex seems to develop from the airfoil leading edge. Downstream, induced vortices are developing on the bottom wall. The longitudinal vorticity components of the tip separation and tip leakage vortices, on one hand, and the induced vortices, on the other hand, are of opposite signs. This indicates opposite direction of rotation between the vortices.

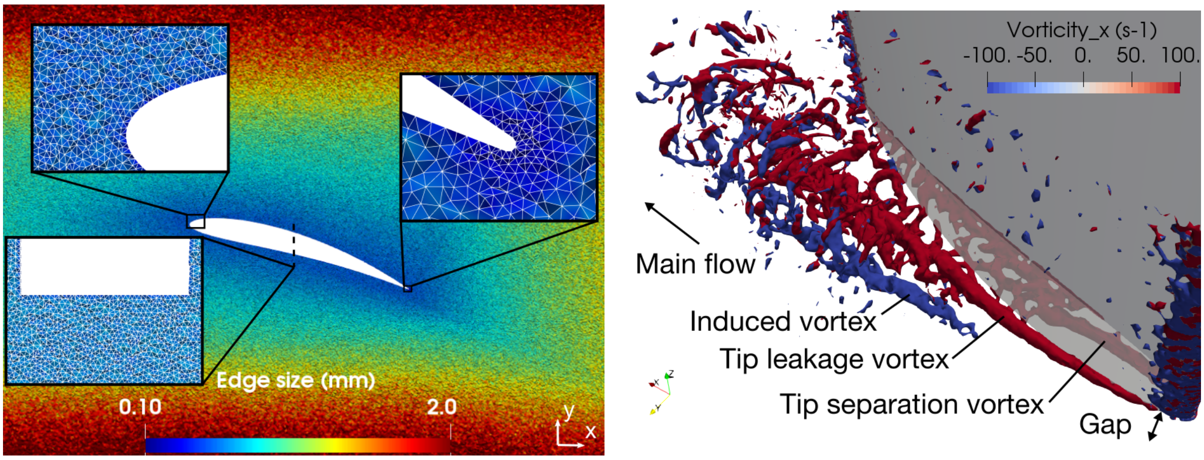

(a)

(b)

Figure 2: **(a) Edge size of the LES mesh around the airfoil at z/s = 2 and close-ups at the airfoil leading and trailing edges and in the gap. (b) LES instantaneous iso-surfaces of Q criterion (Q = 2.4 x 10^2 $(U_0/c)^2$) colored by the longitudinal vorticity component in the tip leakage flow region.**

MEAN FLOW

Flow field of the airfoil-freejet facility

Fig. 3 shows a slice of the mean velocity field close to the tip (z/s = 2) extracted from the RANS simulation (left) and the LES (right). On the RANS field (left), two mixing layers developed from the convergent exit section are observed. When reaching the airfoil leading edge (x/c = -1), the rectangular jet is clearly deflected by the circulation generated by the airfoil. Lobes of velocity around the airfoil interact with the mixing layers at x/c = -0.5, y/c = $\pm$1. This results in a modification of the pressure distribution on the airfoil. Moreover, a deficit of velocity magnitude is observed at y/c = 0.25, from x/c = 0. It corresponds to the trajectory of the tip leakage vortex. At x/c = 1.5, the vicinity of the mixing layers seems to modify the trajectory of the tip leakage vortex and will most likely influence its dynamics. The airfoil wake is also clearly identified next to the tip leakage vortex. All these observations confirm the necessity to include the jet in the simulations.

The LES field (right) is rather similar to the RANS one. Lobes of velocity around the airfoil are identical. The jet deviation for the LES (8°) is less important than for the RANS computation (14°). This shows the capacity of the computational approach to account for the airfoil-jet interaction. A difference is noted for the tip leakage vortex at x/c=0, y/c=0.25. A more complex structure is observed in the LES compared to the RANS computation. The tip leakage vortex will be deeply studied in a following section.

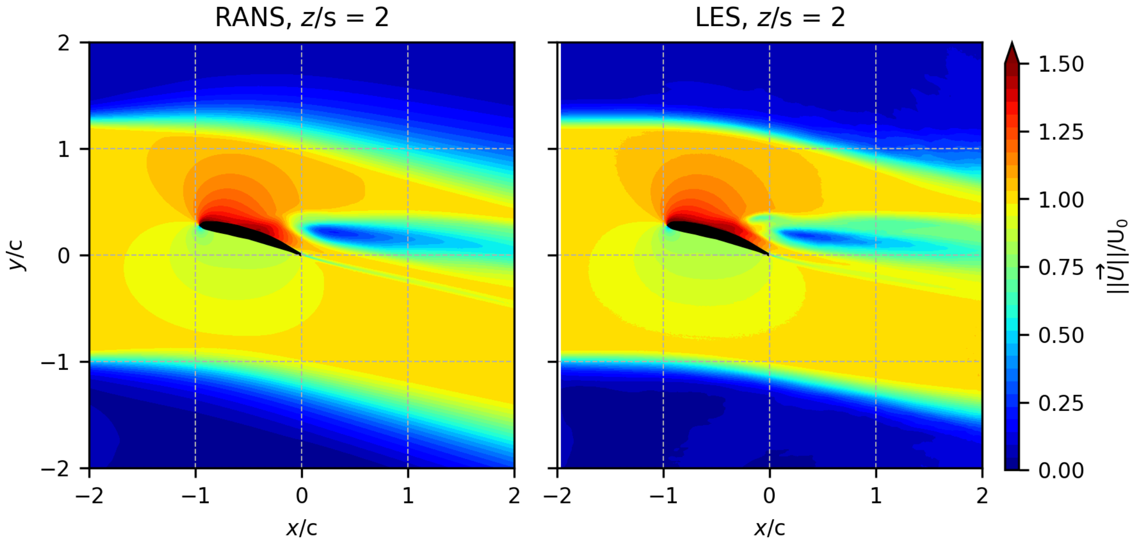

Figure 3: **Mean velocity field close to the tip (z/s = 2) from RANS simulation (left) and LES (right).**

Incoming flow

The mean velocity profile measured with a hotwire probe at (x-x$_{LE}$)/c = -0.50 with x$_{LE}$, the x coordinate of the leading edge, is plotted in Fig. 4a. RANS and LES results are also plotted. Wall-resolved LES from Koch et al. (2020) is labeled by "KOCH". The velocity is normalized by the maximum velocity U$_{max}$ at this axial position. Whereas similar results are obtain by each approach in the inviscid region, some slight discrepancies are observed in the viscous part of the boundary layer. These changes are attributed to the influence of the mesh resolution and the wall law.

Airfoil pressure distribution

Fig. 4b presents the mean pressure coefficients at midspan (z/s = 9) in black and close to the tip (z/s = 0.1) in red. The following definition of pressure coefficient is used: $C_p = (p{-}\mathrm{p}_0)/0.5\rho_0\mathrm{U}_0^2$. The x_c coordinate is defined as: x_c = (x-x$_{LE}$)/(c.cos(β)).

The pressure distributions at midspan in black lines and circles are first considered. The RANS solution is in good overall agreement with the experiment. A slight deviation is observed on the suction side, close to the leading edge (upper solid black line for $x_c < 0.2$). The pressure distribution from LES perfectly matches the RANS one. Therefore, the same conclusions as for the RANS simulation can be done. Wall-resolved LES from Koch et al. (2020) exhibits the same shape of the distribution but closer to the measurement. It is explained by a different angle of attack in the wall-resolved LES (15°). The numerical pressure distributions at midspan globally match the measurement, attesting for a correct operating point.

The pressure distributions close to the tip in red are now analysed. The measured airfoil loading (red circles) is globally reduced compared to the one at midspan. The tip leakage flow from the pressure side to the suction side partially balances the pressure difference. Moreover, the pressure on the suction side (upper red circles) for $0.2 < x_c < 0.8$ is reduced compared to the pressure at midspan because of the presence of the tip leakage vortex. This hump of pressure

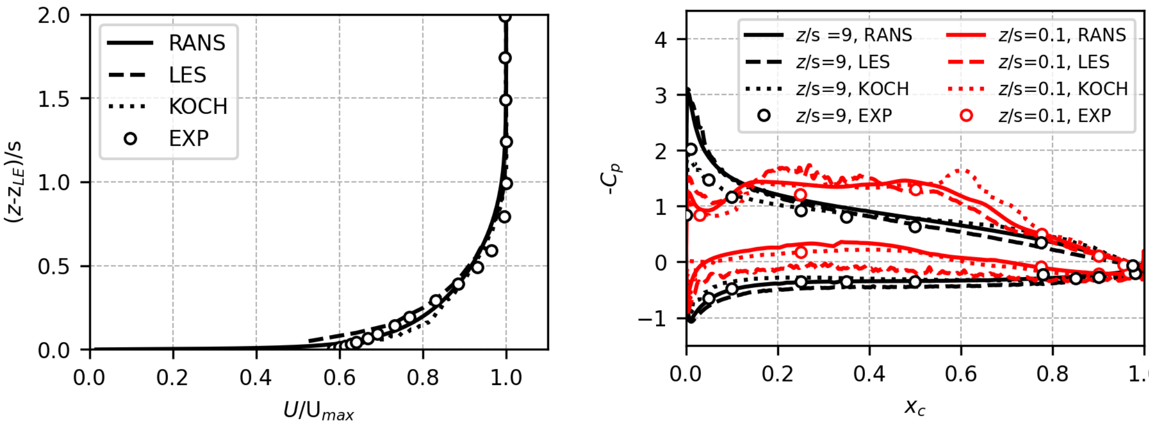

(a) (b)

Figure 4: **(a) Mean velocity profiles normalized by U_{max} at (x-x_{LE})/c= -0.5 for the experiment, RANS simulation, LES and Koch et al. (2020). (b) Mean pressure coefficients at midspan (z/s = 9) in black and close to the tip (z/s = 0.1) in red, for the experiment, RANS simulation, LES and Koch et al. (2020).**

is more or less important depending on the position of the tip leakage vortex relatively to the airfoil (Storer & Cumpsty 1991). The RANS results match well the experimental data on both sides. The pressure distribution from LES almost matches the measurements. In addition, the LES globally matches Koch's results showing the capacity of the wall law to model the flow on the airfoil tip. On the pressure side (lower red lines), the LES predicts higher values of pressure compared to the RANS simulation. The pressure difference at the airfoil tip is responsible for the generation of the tip leakage flow. Therefore the global agreement of pressure distributions close to the tip is attesting for a correct prediction of the tip leakage flow by the RANS simulation and by the LES.

Tip leakage vortex

Fig. 5 shows the longitudinal (up), horizontal (middle) and vertical (down) mean velocity components of the tip leakage vortex at the airfoil trailing edge (x/c = 0.01) for the PIV measurements (left), the RANS simulation (middle), and the LES (right). Since the tip leakage vortex is roughly aligned with the **x** axis (Fig. 3), the considered plane is almost perpendicular to the trajectory of the tip leakage vortex. The flow fields are viewed from downstream. The velocity components are normalised by the reference mean velocity U_0.

The horizontal and vertical mean velocity components V and W corresponding to the middle and lower parts of Fig. 5 are first analysed together. Looking at the PIV measurements on Fig. 5d and 5g, a region of positive V is observed for z/s < 1 whereas a region of negative V is shown for z/s > 1. For the vertical mean component W, two regions are also identified: positive W for y/s > 4 and negative W for y/s < 4. This clearly shows the roll up of the tip leakage vortex. The same kind of flow topology is remarkable around y/s = 7 but with a smaller spatial extension and opposite signs compared to the tip leakage vortex. This flow topology indicates an induced vortex. In addition, for the horizontal component V, the extension of the region in red (z/s$<$ 0) in the gap brings out the jet-like tip leakage flow. The RANS simulation, on Fig. 5e and 5h, correctly reproduces the topology of the tip leakage flow region but diffusion

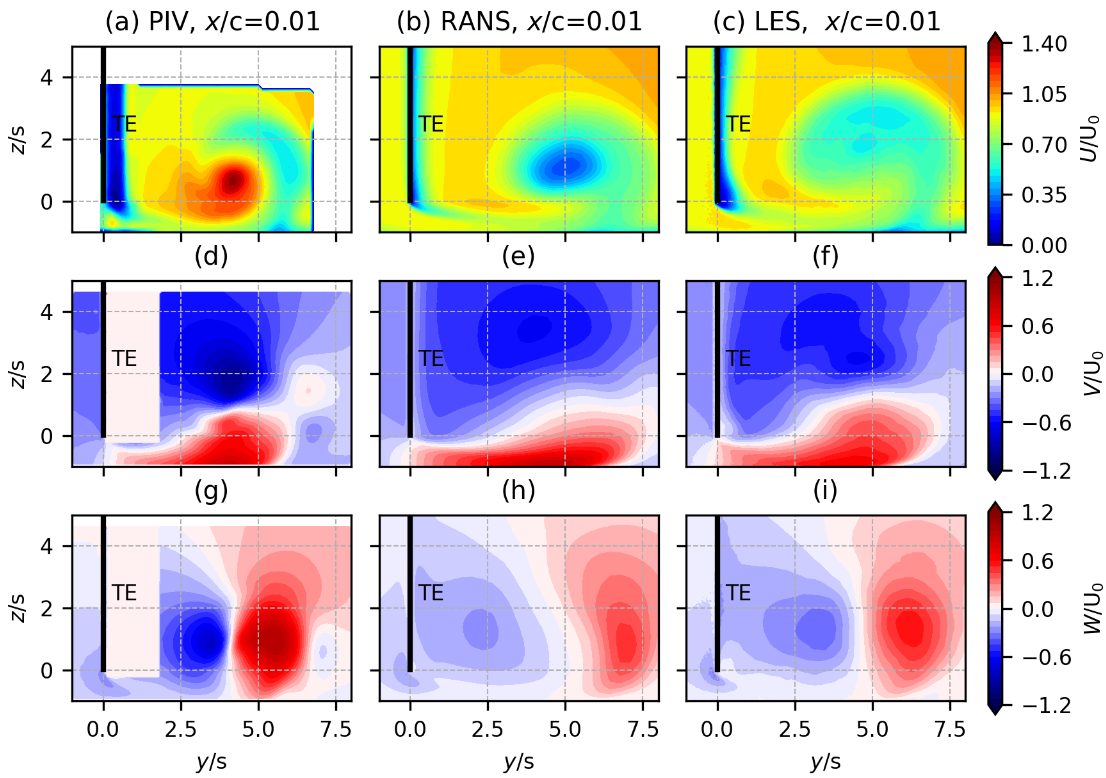

Figure 5: **Longitudinal (up), horizontal (middle) and vertical (down) mean velocity components of the tip leakage vortex at the airfoil leading edge (x/c = 0.01) for the PIV measurements (left), the RANS simulation (middle), and the LES (right).**

is noted. Indeed, a lower velocity magnitude is observed and the tip leakage vortex is much more spatially spread out compared to the PIV measurements. This is even more pronounced for the vertical component W. The LES, on Fig. 5f and 5i, also reproduces the topology of the tip leakage vortex. Diffusion is less important compared to RANS. This may be explained by the order of the convection scheme and the RANS model. Indeed, a second order scheme is used for the RANS whereas a third order scheme is employed for the LES. Moreover, the $k-\omega$ Wilcox model is much more suited to wall bounded flow than to free shear flow. Looking at the vertical velocity component W, the center of the tip leakage vortex is identified by the sudden change of sign. In the PIV measurement, the center is at y/s = 4, whereas for RANS and LES, it is at y/s = 5. Thus, the tip leakage vortex in the simulations is one gap height farther away from the airfoil compared to measurements. This may be a consequence of the early detachment of the tip leakage vortex from the airfoil. Indeed, when the vortex detaches, it starts to move away from the airfoil.

The longitudinal mean velocity component U of the tip leakage vortex corresponding to the upper part of Fig. 5 is now studied. On the PIV data (Fig. 5a), two regions of U are identified. A strong acceleration with a maximum of $1.4U_0$ is measured at y/s = 4 and z/s = 1. This position corresponds to the center of the tip leakage vortex. Moreover, a low velocity region surrounding the zone of acceleration extends from the plate until z/s = 3. The latter is generated by the detachment of the plate boundary layer by the tip leakage flow. The RANS results on

Fig. 5b exhibit a different topology with only one low velocity region. The spatial extension of this region in the RANS velocity field corresponds to the sum of the two regions on the PIV field. The minimum of U on the RANS result is equal to $0.3U_0$ and corresponds to the center of the tip leakage vortex. The LES on Fig. 5c predicts a topology that is different from the two others. Indeed, the LES tends to recover the two regions. Nevertheless, velocity magnitudes are lower than the measured ones. This deviation is attributed to the numerical diffusion linked to mesh resolution. The longitudinal velocity component at the center of the tip leakage vortex is equal to $0.7U_0$. Fig. 5 is consistent with Fig. 3 which shows a cut plane at z/s = 2. The LES exhibits a more complex structure compared to the RANS simulation.

PRESSURE FLUCTUATIONS

Fig. 6 presents the pressure spectra on the airfoil suction and pressure sides (left) and on the tip and lower plates (right), at $x_c = (x\text{-x}_{LE})/(\text{c.cos}(\beta))$ = 77.5% for the measurements, the LES and the wall-resolved LES from Koch et al. (2020). For these probes, the experimental data is extracted from Jacob et al. (2010). The experimental cut-off frequency is 22 kHz but data are only available till 10 kHz. The wall-modelled LES cut-off frequency is 5.0×10^4 Hz.

On measured sprectra, a hump around 1.2 kHz is identified for the pressure side, tip and plate probes. However, this hump is not found on the suction side probe. Moreover, the levels of pressure fluctuation are higher for the probes in the gap (tip and plate) compared to the one on the pressure side. Grilliat et al. (2007) explain that this hump characterises the pressure fluctuations induced by the detachment of the tip leakage flow on the airfoil pressure side-tip corner. In addition, the levels of pressure fluctuations on the suction side are higher than those on the pressure side for all frequencies. This is due to the turbulent activity of the tip leakage vortex. For the probes in the gap, the levels are higher on the tip surface compared to the plate surface because the tip leakage flow is fully detached from the airfoil tip.

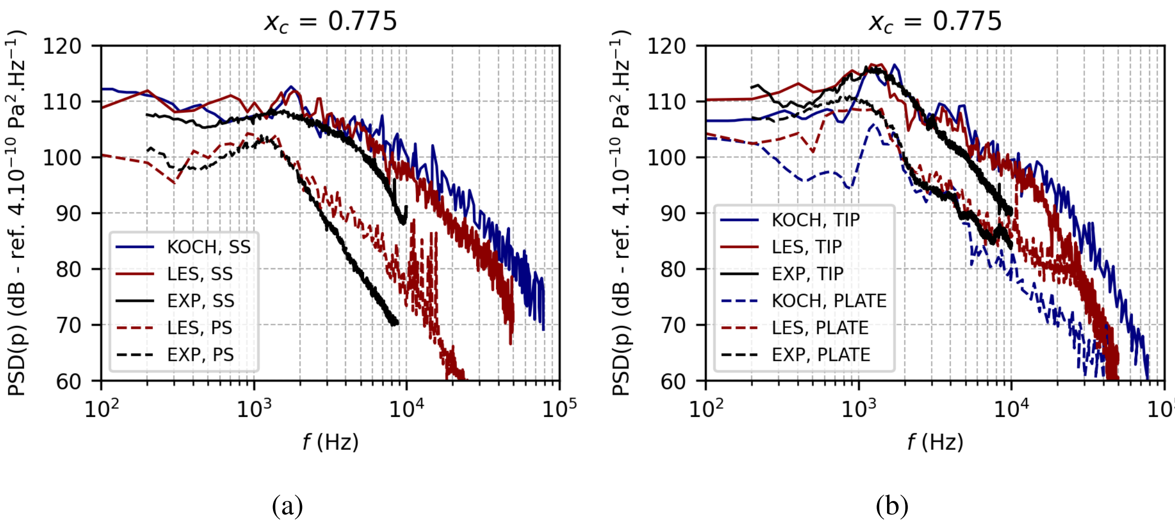

Figure 6: **(a) Pressure spectra on the airfoil suction side (SS) in solid lines and pressure side (PS) in dashed lines at x_c = 77.5% (b) Pressure spectra on the airfoil tip (TIP) in solid lines and on the lower plate (PLATE) in dashed lines at x_c = 77.5%.**

The spectrum from the LES exhibits a good agreement with the experiment in both shape and level. The hump around 1.2 kHz is well reproduced by the simulation: both the central frequency and the amplitude are predicted. Deviations are observed in the spectrum slope for frequencies higher than 3 kHz on the pressure side and tip spectra. In addition, on the pressure side spectrum, tonal signature between 10 and 20 kHz is assumed to be generated by the injection of turbulence at the inlet boundary condition. The wall-modelled LES exhibits globally the same results than the wall-resolved LES and is even better on the plate at low frequency (Fig. 6b). This comparison demonstrates the capacity of the wall law in the frame of the tip leakage flow.

A Dynamic Mode Decomposition (DMD) is applied on the tip leakage flow region. Fig. 7 presents isosurfaces of pressure fluctuations for the DMD mode at the frequency 1341 Hz viewed from the upper plate (a) and the lower plate (b). The blue and red isosurfaces brings out the spatial pattern of pressure fluctuations of the flow for the considered frequency. The surfaces originate from the airfoil pressure side-tip corner. Then, they are convected by the mean flow and roll up around the tip leakage vortex. This confirms that the hump around 1.2 kHz found on wall pressure fluctuations spectra (Fig. 6) are due to turbulent structures generated by the detachment of the tip leakage flow in the gap.

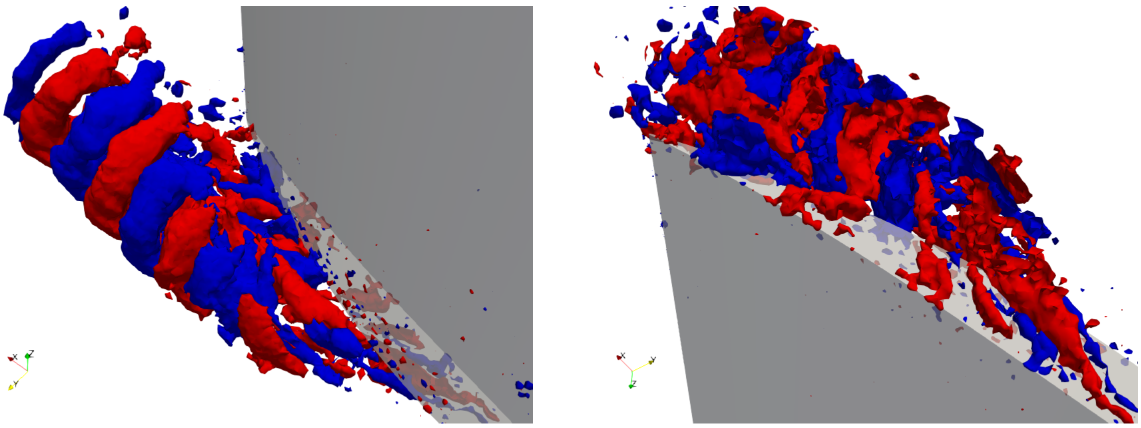

(a) (b)

Figure 7: **Isosurfaces of pressure fluctuations for the DMD mode at the frequency 1341 Hz viewed from the upper plate (a) and the lower plate (b). Blue surfaces are for pressure fluctuations below -100 Pa and red surfaces for those over +100 Pa.**

CONCLUSIONS

The aim of this paper was to evaluate the capabilities of RANS and LES, with respect to experimental data, to compute the aerodynamics of the tip leakage flow. A fixed single airfoil with a gap between the airfoil tip and the lower plate was considered. A computational approach accounting for wind tunnel installation effect was presented. The numerical incoming flow, airfoil pressure distribution, tip leakage vortex and pressure fluctuations in the tip region were compared to experimental data.

The shape of the mean velocity profile was well predicted by both simulations. The pressure distribution at midspan was well reproduced in the simulations. This demonstrates the correct simulation of the airfoil-jet interaction. Moreover, the influence of the tip leakage flow and vortex on the pressure distribution at the tip was also well captured. The mean aerodynamics of the tip leakage vortex was globally predicted by the simulations. The numerical tip leakage vortex were a bit wider and farther away from the airfoil. LES with mesh refinement inside the tip leakage vortex is currently performed to improve the prediction of the longitudinal component. Unlike the RANS method, the LES managed to compute a more complex structure of the tip leakage vortex justifying the use of this method. Finally, the spectral content of the wall pressure fluctuations in the tip region was correctly computed. As a consequence the wall-modelled approach is validated to study this type of flow as it compares well with both wall-resolved LES and experiment. A Dynamic Mode Decomposition was applied on the tip leakage flow region. It was confirmed that the hump around 1.2 kHz on the wall pressure spectra are due to turbulent structures generated by the detachment of the tip leakage flow in the gap.

Resorting to the LES is essential for the intended future acoustic applications, details of which are beyond the scope of the present paper. Indeed, explicit wall-pressure statistics requiring the simulation of the turbulence are generally used as input data in the sound prediction models.

ACKNOWLEDGEMENTS

This study has been co-funded by Safran Aircraft Engines and ANRT through a CIFRE PhD thesis. This work was performed within the framework of the LABEX CeLyA (ANR-10-LABX-0060) of Université de Lyon, within the program "Investissements d'Avenir" (ANR-16-IDEX-0005) operated by the French National Research Agency (ANR). The authors are grateful for the experimental data provided by Emmanuel Jondeau from the *Laboratoire de Mécanique des Fluides et d'Acoustique* de l'*École Centrale de Lyon*. This work was granted access to the HPC resources of TGCC under the allocation A0082A06074 made by GENCI.

REFERENCES

Cambier, L., Heib, S. & Plot, S. (2013), 'The Onera elsA CFD software: input from research and feedback from industry', *Mechanics & Industry* **14**(3), 159–174.

Colin, O. & Rudgyard, M. (2000), 'Development of high-order Taylor–Galerkin schemes for LES', *Journal of Computational Physics* **162**(2), 338–371.

Daviller, G., Oztarlik, G. & Poinsot, T. (2019), 'A generalized non-reflecting inlet boundary condition for steady and forced compressible flows with injection of vortical and acoustic waves', *Computers & Fluids* **190**, 503–513.

Fukano, T. & Jang, C. M. (2004), 'Tip clearance noise of axial flow fans operating at design and off-design condition', *Journal of Sound and Vibration* **275**(3-5), 1027–1050.

Grilliat, J., Jacob, M., Camussi, R. & Caputi-Gennaro, G. (2007), Tip leakage experiment-part one: Aerodynamic and acoustic measurements, *in* '13th AIAA/CEAS Aeroacoustics Conference (28th AIAA Aeroacoustics Conference)', p. 3684.

Jacob, M. C., Grilliat, J., Camussi, R. & Gennaro, G. C. (2010), 'Aeroacoustic Investigation of a Single Airfoil Tip Leakage Flow', *International Journal of Aeroacoustics* **9**(3), 253–272.

Jacob, M. C., Jondeau, E. & Li, B. (2016), 'Time-resolved PIV measurements of a tip leakage flow', *International Journal of Aeroacoustics* **15**(6-7), 662–685.

Kameier, F. & Neise, W. (1997), 'Experimental Study of Tip Clearance Losses and Noise in Axial Turbomachines and their Reduction', *Journal of Turbomachinery* **119**(3), 460–471.

Koch, R., Sanjose, M. & Moreau, S. (2020), Large-eddy simulation of a single airfoil tip-leakage flow, *in* 'AIAA AVIATION 2020 FORUM', p. 2514.

Kraichnan, R. H. (1970), 'Diffusion by a random velocity field', *The physics of fluids* **13**(1), 22–31.

Lakshminarayana, B. (1996), *Fluid Dynamics and Heat Transfer of Turbomachinery*, John Wiley & Sons Inc.

Longhouse, R. E. (1978), 'Control of tip-vortex noise of axial flow fans by rotating shrouds', *Journal of Sound and Vibration* **58**(2), 201–214.

Moreau, S., Henner, M., Iaccarino, G., Wang, M. & Roger, M. (2003), 'Analysis of flow conditions in freejet experiments for studying airfoil self-noise', *AIAA journal* **41**(10), 1895–1905.

Nicoud, F., Toda, H. B., Cabrit, O., Bose, S. & Lee, J. (2011), 'Using singular values to build a subgrid-scale model for large eddy simulations', *Physics of Fluids* **23**(8), 085106.

Passot, T. & Pouquet, A. (1987), 'Numerical simulation of compressible homogeneous flows in the turbulent regime', *Journal of Fluid Mechanics* **181**, 441–466.

Poinsot, T. & Lele, S. (1992), 'Boundary conditions for direct simulations of compressible viscous flows', *Journal of computational physics* **101**(1), 104–129.

Roe, P. L. (1981), 'Approximate Riemann solvers, parameter vectors, and difference schemes', *Journal of computational physics* **43**(2), 357–372.

Schmitt, P., Poinsot, T. & Schuermans, B .and Geigle, K. (2007), 'Large-eddy simulation and experimental study of heat transfer, nitric oxide emissions and combustion instability in a swirled turbulent high-pressure burner', *Journal of Fluid Mechanics* **570**, 17–46.

Schønfeld, T. & Rudgyard, M. (1999), 'Steady and unsteady flow simulations using the hybrid flow solver AVBP', *AIAA journal* **37**(11), 1378–1385.

Storer, J. A. & Cumpsty, N. A. (1991), 'Tip Leakage in Axial Compressors', *Journal of Turbomachinery* **113**(2), 252.

Wang, M., Moreau, S., Iaccarino, G. & Roger, M. (2009), 'LES prediction of wall-pressure fluctuations and noise of a low-speed airfoil', *International journal of aeroacoustics* **8**(3), 177–197.

Wilcox, D. C. (1988), 'Reassessment of the scale-determining equation for advanced turbulence models', *AIAA journal* **26**(11), 1299–1310.

You, D., Wang, M., Moin, P. & Mittal, R. (2007), 'Large-eddy simulation analysis of mechanisms for viscous losses in a turbomachinery tip-clearance flow', *Journal of Fluid Mechanics* **586**, 177–204.

Zheng, X. & Liu, F. (1995), 'Staggered upwind method for solving Navier-Stokes and k-omega turbulence model equations', *AIAA journal* **33**(6), 991–998.